EPJ Web of Conferences **366**, 01005 (2026) https://doi.org/10.1051/epjconf/202636601005
10th Complexity-Disorder Days 2025

Is the hyperscaling relation violated below the upper critical dimension in some particular cases?

H. T. Diep[1,*] and *Van-Thanh* Ngo[2,**]

[1]Laboratoire de Physique Théorique et Modélisation, CY Cergy Paris Université, CNRS, UMR 8089
2, Avenue Adolphe Chauvin, 95302 Cergy-Pontoise, France.
[2]Institute of Scientific Data and Information, Vietnam Academy of Science and Technology (VAST)
18 Hoang Quoc Viet, Hanoi 10000, Vietnam.

Abstract. In this paper, we review our recent results on the critical exponents of thin films obtained by high-performance multi-histogram Monte Carlo simulations. This review shows that the critical exponents do not satisfy the hyperscaling relation. The film thickness N_z consists of a few layers up to a dozen of layers in the z direction. The free boundary condition is applied in this direction while in the xy plane periodic boundary conditions are used. We also show the cross-over between the first- and second-order transition while decreasing the film thickness in a frustrated thin film. In the third case, we show evidence that when a 2D system has two order parameters of different symmetries, the critical exponents break the hyperscaling. The last case is the 3D Ising model coupled to the lattice vibration: the results also suggest the violation of the hyperscaling.

1 Introduction

The study of phase transitions is one of the most important tasks in theory, in experiments and in computer simulations since the second half of the 20th century. The main reason is that, if we know the characteristics of a phase transition, we can understand the interaction mechanisms lying behind the transition and we can deduce various physical quantities. Therefore, comparisons between theories, experiments and computer simulattions are necessary in order to obtain conclusions. While comparison with experiments is always a challenge because real materials may contain ill-controlled elements such as dislocations, defects and impurities, comparisons between theories and simulations are in most cases possible. This is the purpose of the present paper revisits our own works in the past 20 years (see our works cited in [1,2]).

Let us recall that the phase transition was first studied by the mean-field approximation with several improved versions in the 40s (see the textbook [3] where these methods are shown and commented). These were followed by exact-solution methods in two dimensions (2D) such as the Ising model, Potts models and vertex models (see the book by R. Baxter [4]). The break-through in general dimensions come in 1970 with the formulation of the renormalization group by K. G. Wilson [5,6] followed by investigations on the finite-size scaling analysis and their validity [7-9]. As known, there are six critical exponents and there are four relations between them. One is called 'hyperscaling relation' connected with the space dimension d. There have been investigations on the progress made on the scaling and hyperscaling relations above the upper critical dimension $d_u = 4$. The reader is referred, for example, to Ref. [10] and the review by Young [11] for a recall of the demonstration of these relations (see also the review by Honchar et al. [12]). It should be added that this violation is explained in the framework of Renormalization-Group theory by the existence of a dangerous irrelevant variable [13]. The main question is whether or not the hyperscaling is violated for dimension d larger than the upper critical dimension $d_u = 4$. In the present paper, however, we show that the question of the violation of the hyperscaling is also posed in $d < 4$ in some specific cases that we will present in this paper. It should be mentioned that Renormalization-Group calculations conclude that the hyperscaling relation should hold for thin films in the case of large-N limit [14]. But in the present paper, we consider thin films of Ising spins ($N = 1$) in section 2, so the result of this paper does not apply.

The first case studied in the present paper concerns the critical exponents obtained by using the highly-precise multi-histogram Monte Carlo (MC) technique [15-17] for a thin film of simple cubic structure with Ising spin model. The film surface L^2 (xy plane) is very large, up to $L^2 = 160^2$ lattice sites for some cases, with periodic boundary conditions, while the film thickness N_z goes from one layer (2D) to 13 layers with free boundary conditions. Finite-size scaling (FSS) has been used with varying L to calculate the critical exponents. These results have been published in Ref. [18] but the aspect of the violation of the hyperscaling relation has not been discussed. In the light of the violation of the hyperscaling relation for $d \geq d_u$ [10,11], we revise the interpretation of our results. In ad-

*e-mail: diep@cyu.fr
**e-mail: nvthanh@vast.vn

dition, we review some other cases that we have investigated.

Except the case $N_z = 1$, the question of the dimension of the system naturally arises. For Capehart and Fisher [19], there is a cross-over from 2D to 3D when N_z is increased. So, how should one use the hyperscaling relation, namely with which dimension ? We will discuss this in this paper.

This paper is organized as follows. Section 2 is devoted to the case of thin films mentioned above where the multi-histogram technique is recalled. Section 3 shows the results of critical exponents obtained with the FSS. Section 4 reviews the case of a cross-over between the first- and second-order transitions when the film thickness of a frustrated antiferromagnetic FCC film is decreased. Section 5 is devoted to some other cases where the hyperscaling relation is violated or seems to be violated. Concluding remarks are given in section 6.

2 Critical Behavior of Thin Films

2.1 Model

We consider a thin film composing of N_z layers of xy square lattices stacking in the z direction. The xy plane has the dimension $L \times L$ where L is the linear dimension. We use a simple Hamiltonian which consists of Ising spins occupying the lattice sites. The spins interact with each other via an exchange interaction J between nearest neighbors (NN). We assume J to be uniform everywhere including between surface spins. The Hamiltonian is written as

$$\mathcal{H} = -J \sum_{i,j} \sigma_i \, \sigma_j. \tag{1}$$

In the simulations which will be shown below, we take N_z from 1 to 13 and $L = 20 - 80$ (for some cases L is up to 160). Before showing our results, let us summarize the multi-histogram technique in the following.

2.2 Multi-histogram Technique

We know that with a finite-size system the maximum of the specific heat C_v and the maximum of the susceptibility χ do not occur at the same temperature. In the first run., using Metropolis algorithm [20], we record the energy histogram $H(E)$. Using the canonical distribution, we calculate C_v and χ as a continuous functions of T. Next, we take a temperature close to the maximum of C_v and the maximum of χ to calculate by histogram technique the new temperatures of the maxima of C_v and χ. We repeat again this procedure for 8 temperatures: such an iteration procedure improves the positions of the maxima of C_v and χ at the system size (L, N_z). The reader is referred to Refs. [16,17] for more technical details. Note that, as in the single histogram technique, thermal physical quantities are calculated as continuous functions of T which allow for the precise determination of the peak positions and the peak heights of C_v and χ for a given system size. This permits making the finite-size scaling with precision. In addition, since we take many temperatures in the transition region, the results obtained by multi-histogram method are valid for a wider range of temperature, unlike a single histogram technique with the results valid only in a very small temperature region, typically $[T - T_c(\infty)]/T_c(\infty) \simeq \pm 1\%$.

The multiple histogram technique reproduces with very high accuracy the critical exponents of second order phase transitions [15-17]. The overall probability distribution [17] at temperature T obtained from n independent simulations, each with N_j configurations, is given by

$$P(E,T) = \frac{\sum_{i=1}^{n} H_i(E) \exp[E/k_B T]}{\sum_{j=1}^{n} N_j \exp[E/k_B T_j - f_j]}, \tag{2}$$

where

$$\exp[f_i] = \sum_E P(E, T_i). \tag{3}$$

The thermal average of a physical quantity A is then calculated by

$$\langle A(T) \rangle = \sum_E A \, P(E,T)/z(T), \tag{4}$$

in which

$$z(T) = \sum_E P(E,T). \tag{5}$$

Thermal averages of physical quantities are thus calculated as continuous functions of T, now the results should be valid over a much wider range of temperature than for any single histogram. In practice, as said above, we use first the standard MC simulations to localize for each size the transition temperatures $T_0^E(L)$ for specific heat and $T_0^m(L)$ for susceptibility. The equilibrating time is from 200000 to 400000 MC steps/spin and the averaging time is from 500000 to 1000000 MC steps/spin. Next, we make histograms at 8 different temperatures $T_j(L)$ around the transition temperatures $T_0^{E,m}(L)$ with 2 millions MC steps/spin, after discarding 1 millions MC steps/spin for equilibrating. Finally, we make again histograms at 8 different temperatures around the new transition temperatures $T_0^{E,m}(L)$ with 2×10^6 and 4×10^6 MC steps/spin for equilibrating and averaging time, respectively. Such an iteration procedure gives extremely good results for systems studied so far. Errors shown in the following have been estimated using statistical errors, which are very small thanks to our multiple histogram procedure, and fitting errors given by fitting software.

In our simulations, the following thermal averages have been recorded
- the magnetization$\langle M \rangle$

$$\langle M \rangle = \frac{1}{L^2 N_z} \langle \sum_i \sigma_i \rangle, \tag{6}$$

- the total energy $\langle E \rangle$,

$$\langle E \rangle = \langle \mathcal{H} \rangle, \tag{7}$$

- the heat capacity C_v,

$$C_v = \frac{1}{k_B T^2} \left(\langle E^2 \rangle - \langle E \rangle^2 \right), \tag{8}$$

- the susceptibility χ,

$$\chi = \frac{1}{k_B T}\left(\langle M^2\rangle - \langle M\rangle^2\right), \tag{9}$$

- the Binder energy cumulant U,

$$U = 1 - \frac{\langle E^4\rangle}{3\langle E^2\rangle^2}, \tag{10}$$

-n^{th} order cumulant of the order parameter V_n for $n = 1$ and 2:

$$V_n = \frac{\partial \ln M^n}{\partial(1/k_B T)} = \langle E\rangle - \frac{\langle M^n E\rangle}{\langle M^n\rangle}. \tag{11}$$

Note that, since N_z is fixed, the following quantities scale with L [11,16,20]:

$$V_1^{\max} \propto L^{1/\nu}, \qquad V_2^{\max} \propto L^{1/\nu}, \tag{12}$$

$$C_v^{\max} = C_0 + C_1 L^{\alpha/\nu} \tag{13}$$

and

$$\chi^{\max} \propto L^{\gamma/\nu}, \tag{14}$$

at their respective 'transition' temperatures $T_c(L)$. Furthermore, we have

$$U = U[T_c(\infty)] + AL^{-\alpha/\nu}, \tag{15}$$

$$M_{T_c(\infty)} \propto L^{-\beta/\nu}, \tag{16}$$

and

$$T_c(L) = T_c(L=\infty) + C_A L^{-1/\nu}. \tag{17}$$

where A, C_0, C_1 and C_A are constants. The exponent ν can be calculated by Eqs. (12). For L large enough, $V_1^{\max}$ and $V_2^{\max}$ should give the same ν as seen below. Then, from Eq. (17) we estimate $T_c(L=\infty)$. Using this, we calculate α and β from Eqs. (15) and (16). We will check the Rushbrooke inequality $\alpha+2\beta+\gamma \geq 2$ and the hyperscaling relation $d\nu = 2-\alpha$ in the following.

In addition, in order to guaranty that Eqs. (12)-(17) are used for L large enough, one uses the following corrections to scaling of the form

$$\chi^{\max} = B_1 L^{\gamma/\nu}(1 + B_2 L^{-\omega}), \tag{18}$$

$$V_n^{\max} = D_1 L^{1/\nu}(1 + D_2 L^{-\omega}), \tag{19}$$

B_1, B_2, D_1 and D_2 being constants and ω a correction exponent [21]. Normally, if L is large enough, the corrections are very small. With today's computer memory capacity, large L is often used as seen below. The scaling corrections are thus extremely small, they do not therefore alter the results using Eqs. (12)-(17).

3 Results

Most of the results shown below have been published by us in [18]. However, in light of the new interpretation on the violation of the hyperscaling relation, we revisit them here to show that there is a possibility that the hyperscaling relation $d\nu = 2-\alpha$ is violated below d_u: as mentioned in the Introduction, in the case of thin films where the thickness is finite and small, the hyperscaling relation is satisfied only when d has a value between 2 and 3. This non-integer dimension is called by Capehart and Fisher [19] "cross-over dimension". To our knowledge, d in the hyperscaling relation is the space dimension, it is 2, 3, ... (integer), it cannot be between 2 and 3. We are convinced that the hyperscaling relation may not be valid in the case of thin films shown below and in other particular cases shown in section 5.

First, we show the layer magnetizations and their corresponding susceptibilities of the first three layers in the case where $N_z = 5, L = 24$ in Fig. 1. The layer susceptibilities have their peaks at the same temperature, indicating a single transition. We note that the magnetization is lowest at the surface and increases while going to the interior. This is known a long time ago by the Green's function method [3,22,23] and by more recent works on thin films with competing interactions [24] and films with Dzyaloshinskii-Moriya interaction [25,26]. Physically, the surface spins have smaller local field due to the lack of neighbors, so thermal fluctuations will reduce more easily the surface magnetization with respect to the interior ones.

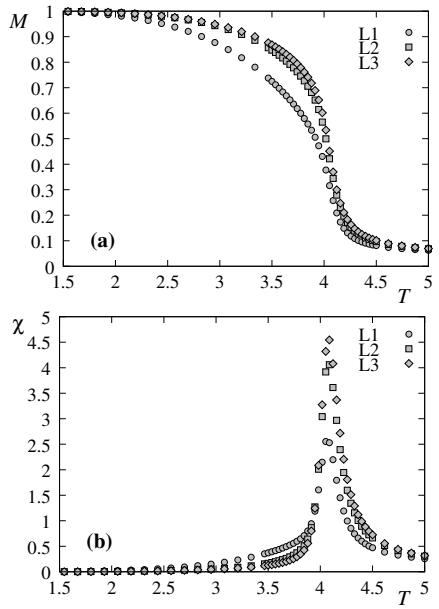

Figure 1. (a) Layer magnetizations of layer 1 (denoted by L_1), layer 2 (denoted by L_2) and layer 3 (denoted by L_3), (b) Layer susceptibilities, as functions of T with $N_z = 5$ and $L = 24$.

We plot in Fig. 2 the total magnetization and the total susceptibility. The latter shows only one peak, signature of a single transition. This justifies the study shown below on the criticality of the film transition.

3.1 Finite size scaling

Let us show our finite-size scaling (FSS) with L varying from 20 to 80. For $N_z = 3$ we use L up to 160 to evaluate the corrections to scaling. The technical details are

described in the subsection 2.2 above. Note that the multi-histograms at 8 temperatures in the critical region have been performed iteratively many times. Such an iteration procedure gives extremely good results. Errors shown in the following have been estimated using statistical errors, which are very small thanks to our multiple histogram procedure, and fitting errors given by fitting software. Note that the errors are at the 3rd digit as seen in Table 1, they are smaller than the size of the data points shown in the figures.

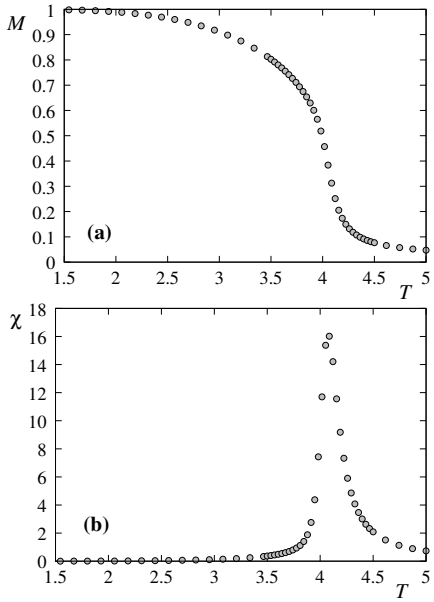

Figure 2. (a) Total magnetization per site, (b) Total susceptibility per site, versus T with $N_z = 5$ and $L = 24$.

3.2 Critical exponents obtained with finite-size scaling

We show first the peak height of the susceptibility and the maximum of V_1 as functions of T for varying L from 20 to 80 in Fig. 3.

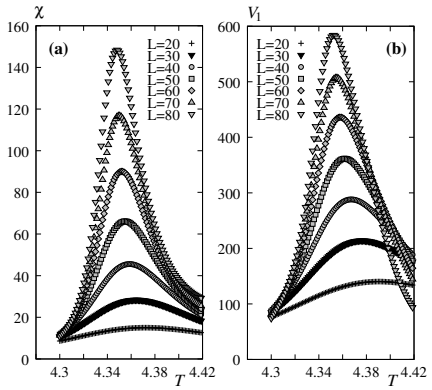

Figure 3. (a) Susceptibility and (b) V_1, as functions of T for $L = 20, 30, ..., 80$ with $N_z = 11$, obtained by multiple histogram technique. Note the strong dependence of the peak height on L.

Note that the results shown below are obtained using $T_c(L = \infty, N_z)$ as described earlier below Eq. (17). We show in Fig. 4 V_1^{max} versus L in the $ln - ln$ scale for $N_Z = 1, 3, ..., 13$. The slope of a given straight line gives $1/\nu$ of the corresponding N_z.

To show the precision of our method, we give here the results of $N_z = 1$. For $N_z = 1$, we have $1/\nu = 1.0010 \pm 0.0028$ which yields $\nu = 0.9990 \pm 0.0031$ and $\gamma/\nu = 1.7537 \pm 0.0034$ and $\gamma = 1.7520 \pm 0.0062$. These results are in excellent agreement with the exact results $\nu_{2D} = 1$ and $\gamma_{2D} = 1.75$. The very high precision of our method is thus verified in the rather modest range of the system sizes $L = 20 - 80$ used in the present work. Note that the result of Ref. [27] gave $\nu = 0.96 \pm 0.05$ for $N_z = 1$ which is very far from the exact value. The results of γ/ν are shown in Figs. 6 and 7. The results of α/ν are shown in Fig. 8. These critical exponents are, although close to those of 2D, show a systematic deviation from the 2D case with increasing N_z.

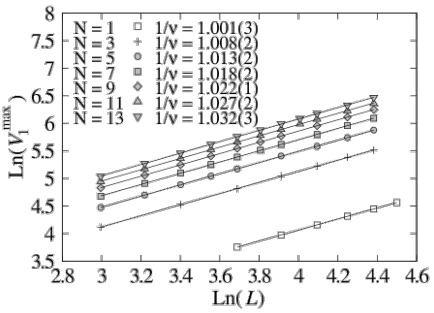

Figure 4. Maximum of V_1 versus L in the ln – ln scale for various N_z. The slopes give $1/\nu$ [see Eq. (12)]. These values are indicated on the figure.

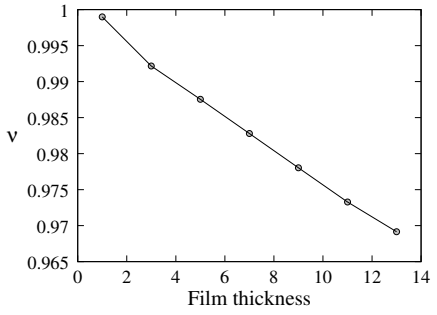

Figure 5. Exponent ν versus N_z. Note that $\nu(2D) = 1$ and $\nu(3D) = 0.62997$.

Exponent ν obtained from Fig. 4 is shown as a function of N_z in Fig. 5

3.3 Corrections to scaling

Let us touch upon the question of corrections to scaling mentioned earlier. We show now that the corrections to scaling are very small. We consider here the effects of larger L and of the correction to scaling for

$N_z = 1, 3, ..., 13$. The results indicate that larger L does not change the results shown above. Figure 9(a) displays the maximum of V_1 as a function of L up to 160. Using Eq. (12), i.e. without correction to scaling, we obtain $1/\nu = 1.009 \pm 0.001$ which is to be compared to $1/\nu = 1.008 \pm 0.002$ using L up to 80. The change is therefore insignificant because it is at the third decimal i. e. at the error level. The same is observed for γ/ν as shown in Fig. 9(b): $\gamma/\nu = 1.752 \pm 0.002$ using L up to 160 instead of $\gamma/\nu = 1.751 \pm 0.002$ using L up to 80.

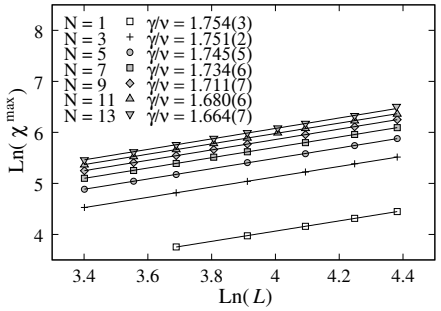

Figure 6. Maximum of susceptibility versus L in the ln – ln scale. The slopes give γ/ν indicated on the figure.

.

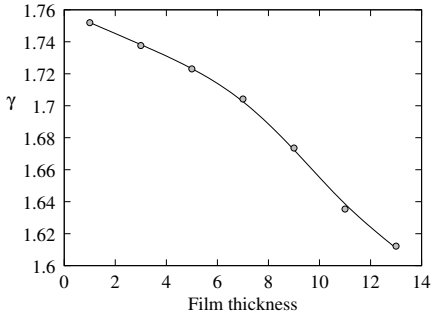

Figure 7. Exponent γ versus film thickness N_z. Note that $\gamma(2D) = 1.75$ and $\gamma(3D) = 1.23707$.

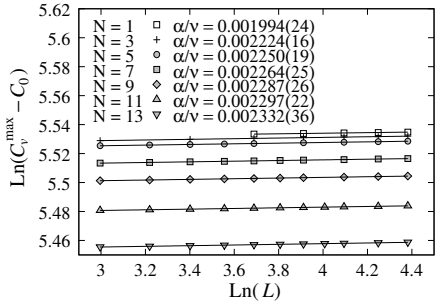

Figure 8. $\ln(C_v^{\max} - C_0)$ versus $\ln L$ for $N_z = 1, 3, 5, ..., 13$. The slope gives α/ν (see Eq. 13) indicated on the figure. Note that $\alpha/\nu(2D) = 0$ and $\alpha/\nu(3D) = 0.110087/0.62997 = 0.174749$.

Now, let us allow for correction to scaling, i. e. we use Eq.(18) instead of Eq. (14) for fitting. We obtain the following values: $\gamma/\nu = 1.751 \pm 0.002$, $B_1 = 0.05676$, $B_2 = 1.57554$, $\omega = 3.26618$ if we use $L = 70$ to 160 (see Fig. 10). The value of γ/ν in the case of no scaling correction is 1.752 ± 0.002. Therefore, we can conclude that this correction is insignificant. The large value of ω explains the smallness of the correction.

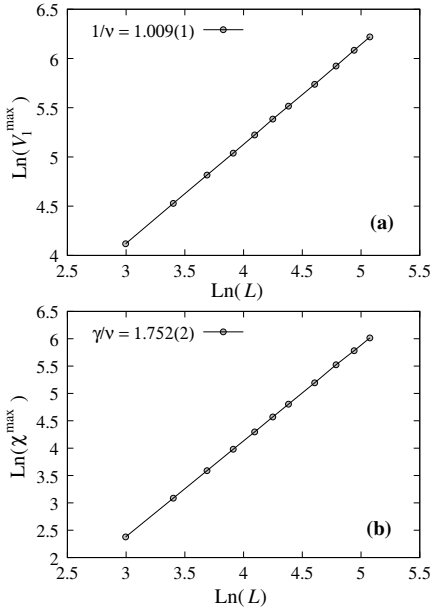

Figure 9. (a) V_1^{max} and (b) χ^{max} vs L in the ln – ln scale for L up to 160 with $N_z = 3$.

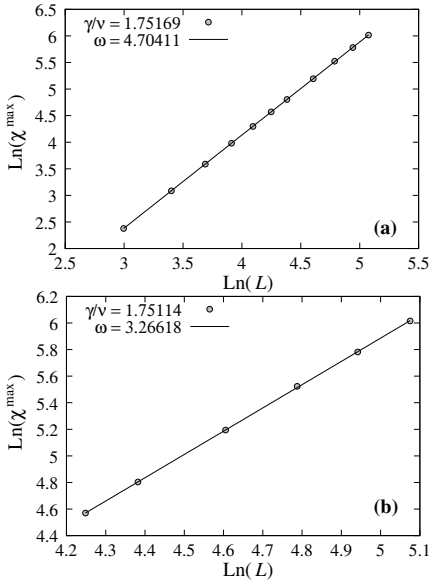

Figure 10. χ^{max} vs L in the ln – ln scale (a) from $L = 20$ up to 160 (b) from $L = 70$ up to 160, for $N_z = 3$.

For β, using Eq. (16) we calculate β/ν for each thickness N_z. The results are precise. For example for N_z=1, we obtained $\beta/\nu = 0.1268 \pm 0.0022$ which yields $\beta = 0.1266 \pm 0.0049$ which is in agreement within errors with

the exact result $\beta = 0.125$. We show in Fig. 11 the exponent β versus N_z.

3.4 Summary of our results

We summarize our results in Table 1. Note that if we use ν and α for a given N_z, except the case $N_z = 1(d = 2)$, the hyperscaling relation $d\nu = 2 - \alpha$ is violated if $d = 2$. This relation is obeyed if the dimension is replaced by an "effective dimension" $d_{\rm eff}$ listed in Table 1 which is a little bit larger than 2. This means that the 2D critical behavior dominates in thin films as expected ($d_{\rm eff}$ varies from 2 to 2.0613 for $N_z = 1$ to 13). The last column shows the critical temperature at $L = \infty$ obtained by using Eq. (17).

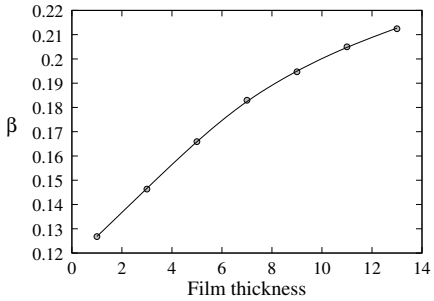

Figure 11. Exponent β as a function of the film thickness N_z.

3.5 Discussion

Let us show in Fig. 12 the effective dimension versus N_z. As seen, though $d_{\rm eff}$ deviates systematically from $d = 2$, its values are however very close to 2. This means that the 2D character is dominant even at $N_z = 13$.

As mentioned above, $d_{\rm eff}$ is very close to 2. However, $T_c(L = \infty, N_z)$ increases very fast to reach a value close to T_c of the 3D Ising model ($\simeq 4.51$) at $N_z = 13$. This is an interesting point. In Ref. [19] Capehart and Fisher define the critical-point shift from the 3D value by

$$\varepsilon(N_z) = \left[T_c(L = \infty, N_z) - T_c(3D)\right] / T_c(3D). \qquad (20)$$

They showed that

$$\varepsilon(N_z) \approx \frac{b}{N_z^{1/\nu}}[1 + a/N_z], \qquad (21)$$

where $\nu = 0.6289$ (3D value). Using $T_c(3D) = 4.51$, we fit the above formula with $T_c(L = \infty, N_z)$ taken from Table 1, we obtain $a = -1.37572$ and $b = -1.92629$. Our results and the fitted curve are shown in Fig. 13. Note that the correction factor $[1 + a/N_z]$ is necessary to obtain a good fit for small N_z. The prediction of Capehart and Fisher is verified by our result.

If the cross-over dimension raised by Capehart and Fisher [19] is identified with the effective dimension between 2 and 3, then the hyperscaling relation involving the space dimension d cannot be satisfied in the case of thin films. Let us take the case $N_z = 13$, we have $d\nu = 2\times0.9692 = 1.9384$, while $2-\alpha = 2-0.00226 = 1.99774$ far from the $d\nu$ value. The hyperscaling relation is thus violated.

We show now that the free boundary condition in the z direction gives the same result, within errors, as the periodic boundary condition (PBC), as far as the critical exponents are concerned. This is shown in Figs. 14 and 15.

We would like to emphasize that the Rushbrooke inequality $\alpha + 2\beta + \gamma \geq 2$ is verified within errors as an equality for each N_z as seen in Table 1.

4 Cross-Over from First- to Second-Order Transition with Varying Film Thickness

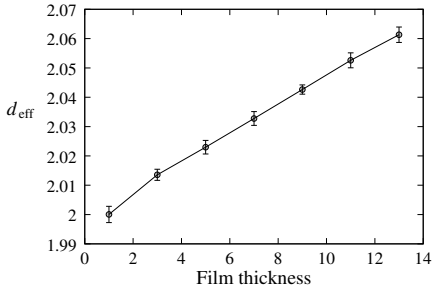

Figure 12. Effective dimension $d_{\rm eff}$ of thin film defined by $d_{\rm eff}\nu = 2 - \alpha$, as a function of thickness N_z. See text for comments.

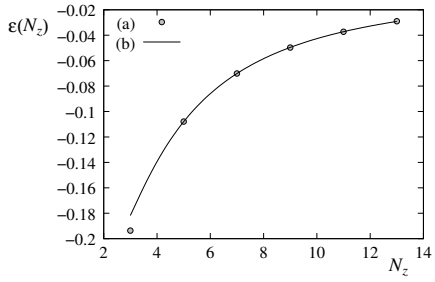

Figure 13. Critical temperature at infinite L, $T_c(L = \infty, N_z)$, versus N_z. MC results are shown by points, continuous line is the prediction of Capehart and Fisher, Eq. (21). The agreement is excellent.

In this section, we show that the film thickness can alter the nature of the transition. We cite here our work on the cross-over between the first- and second-order transition when the film thickness of a fully frustrated FCC antiferromagnet with Ising spins is decreased to ≤ 4 layers (two FCC cells) [28]. We used the highly efficient Wang-Landau method [29-35] to detect the thickness where the first-order transition becomes a second-order one.

Figure 16 shows the strong first-order character of the transition with an energy discontinuity in the bulk case.

In the case of a thin film composed of 8 layers (N_z=4 FCC cells in the z direction), the first-order character remains as shown in Fig. 17 with a double-peak structure.

N_z	ν	γ	α	β	d_{eff}	$T_c(L=\infty, N_z)$
1	0.9990 ± 0.0028	1.7520 ± 0.0062	0.00199 ± 0.00279	0.1266 ± 0.0049	2.0000 ± 0.0028	2.2699 ± 0.0005
3	0.9922 ± 0.0019	1.7377 ± 0.0035	0.00222 ± 0.00192	0.1452 ± 0.0040	2.0135 ± 0.0019	3.6365 ± 0.0024
5	0.9876 ± 0.0023	1.7230 ± 0.0069	0.00222 ± 0.00234	0.1639 ± 0.0051	2.0230 ± 0.0023	4.0234 ± 0.0028
7	0.9828 ± 0.0024	1.7042 ± 0.0087	0.00223 ± 0.00238	0.1798 ± 0.0069	2.0328 ± 0.0024	4.1939 ± 0.0032
9	0.9780 ± 0.0016	1.6736 ± 0.0084	0.00224 ± 0.00161	0.1904 ± 0.0071	2.0426 ± 0.0016	4.2859 ± 0.0022
11	0.9733 ± 0.0025	1.6354 ± 0.0083	0.00224 ± 0.00256	0.1995 ± 0.0088	2.0526 ± 0.0026	4.3418 ± 0.0032
13	0.9692 ± 0.0026	1.6122 ± 0.0102	0.00226 ± 0.00268	0.2059 ± 0.0092	2.0613 ± 0.0027	4.3792 ± 0.0034

Table 1. Critical exponents obtained by multti-histogram technique. The effective dimension and critical temperature $T_c(L=\infty, N_z)$ are listed in the last two columns. See text for the definition of the effective dimension d_{eff}.

We have fitted ΔE with the following function

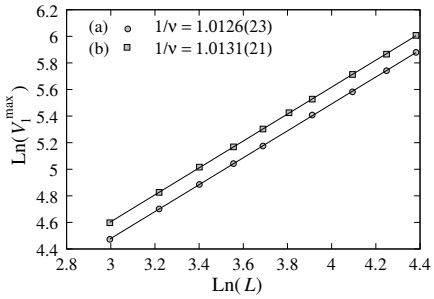

Figure 14. Maximum of V_1 versus L in the ln – ln scale for $N_z = 5$: (a) without PBC in z direction (b) with PBC in z direction. The slopes are indicated on the figure.

$$\Delta E = A - \frac{B}{N_z^{d-1}}\left[1 + \frac{C}{N_z}\right], \tag{22}$$

where $d = 3$ is the space dimension, $A = 0.3370$, $B = 3.7068$, $C = -0.8817$. The second term in the brackets corresponds to a size correction. As seen in Fig. 18, the latent heat vanishes at a thickness $L_z = 2N_z = 4$. This is verified by our simulations for a 4-layer film: the transition has a continuous energy across the transition region, even when $L = 150$.

The energy versus T for $L_z = 4$ is shown in Fig. 19.

As seen in Fig. 20, there are two close transitions: transition of the surface layers at $z = 0$ and $z = 3/2$, and that of the beneath layers at $z = 1/2$ and $z = 1$ (the lattice constant is taken to be 1).

The surface layer has larger magnetization than that of the second layer unlike the non-frustrated case shown in the previous section. One can explain this by noting that due to the lack of neighbors, surface spins are less frustrated than the interior spins, making them more stable than the interior spins. This has been found at the surface of the frustrated helimagnetic film [24]. In order to find the nature of these transitions, using the Wang-Landau technique we study the finite-size effects which are shown in in Figs. 21 and 22. The first peak at $T_1 \simeq 1.927$ corresponds to the vanishing of the second-layer magnetization, it does not depend on the lattice size, while the second peak at $T_2 \simeq 1.959$, corresponding to the disordering of the two surface layers, it depends on L. The histograms shown in Fig. 23 are taken at and near the transition temperatures show a Gaussian distribution indicating a non first-order transition.

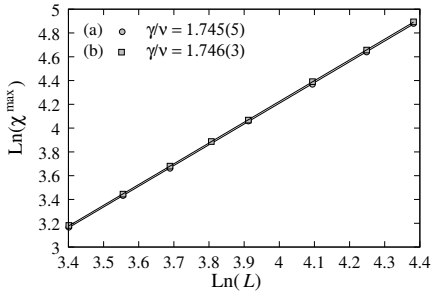

Figure 15. $\chi^{\max}$ versus L in the ln – ln scale for $N_z = 5$ (a) without PBC in z direction (b) with PBC in z direction. The data points of two cases are not distinguishable in the figure scale. The slopes are indicated on the figure.

When we decrease the film thickness, the latent heat goes to zero at 4 layers (i. e. $N_z = 2$) as shown in Fig. 18.

The fact that the peak at T_1 of the specific heat does not depend on L suggests two scenarios: i) T_1 does not correspond to a transition, ii) T_1 is a Kosterlitz-Thouless transition. We are interested here in the size-dependent transition at T_2. Using the multi-histogram technique, we have obtained $\nu = 0.887 \pm 0.009$ and $\gamma = 1.542 \pm 0.005$ for the case of a 4-layer film (see Figs. 24 and 25). These values do not correspond neither to 2D nor 3D Ising models $\nu(2D) = 1$, $\gamma(2D) = 1.75$, $\nu(3D) = 0.63$, $\gamma(3D) = 1.241$. We can interpret this as a dimension cross-over between $2D$ and $3D$. Note that the values we have obtained $\nu = 0.887 \pm 0.009$ and $\gamma = 1.542 \pm 0.005$ belong to a new, unknown universality class. At the time of our work [18], we relied on the hyperscaling relation with $d = 2$ to deduce critical exponent α and using the Rushbrooke equality to calculate β. However, in view of a possible violation of the hyperscaling when d is not the space dimension, we cannot conclude without a direct calculation of α as we have done in the previous section.

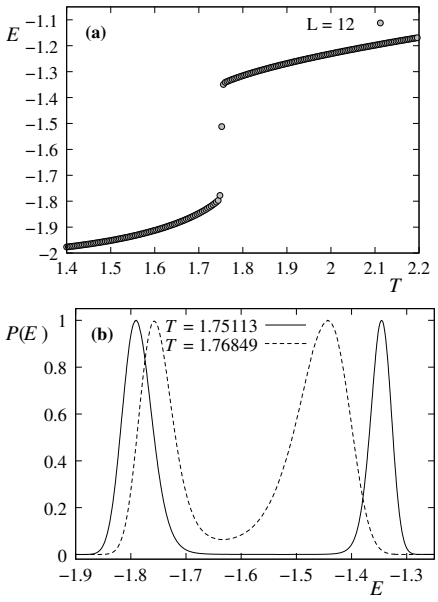

Figure 16. (a) Energy of the bulk case vs T for $L \times L \times L = 12^3$ FCC cells, i. E. the number of spins is $4L^3$; (b) Energy histogram with periodic boundary conditions in all three directions (continuous line) and without PBC (dotted line) in z direction. The histogram was recorded at the transition temperature T_c for each case (indicated on the figure).

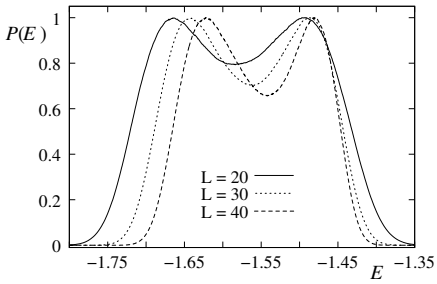

Figure 17. Energy histogram for $L = 20,\ 30,\ 40$ with film thickness of 8 atomic layers at $T = 1.8218,\ 1.8223,\ 1.8227$, respectively.

5 Other cases violating the hyperscaling relation ?

There are cases where the systems have an additional degree of freedom distinct from the order parameter. This is the case of XY spins with a chirality symmetry: while the chiral symmetry can be mapped onto an Ising-like symmetry, the continuous nature of XY spins affects the criticality of the Ising symmetry breaking. Another case is a system of Ising spins in which each spin moves around its lattice site, a kind of magneto-elastic coupling. These two cases have been previously studied [36,45,46]. We briefly show these results below under the view angle of new universality class and the violation or not of the hyperscaling relation below $d_u = 4$.

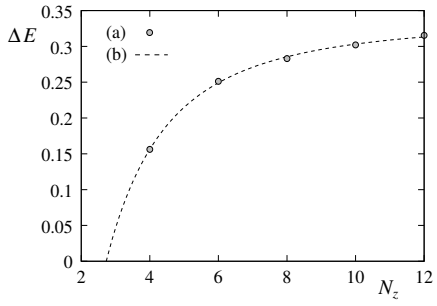

Figure 18. The latent heat ΔE as a function of thickness $L_z = 2N_z$ (points are MC results). The latent heat goes to zero at $N_z = 2$, i.e. at $L_z = 4$ atomic layers. The continuous line is the fitted function Eq . (22).

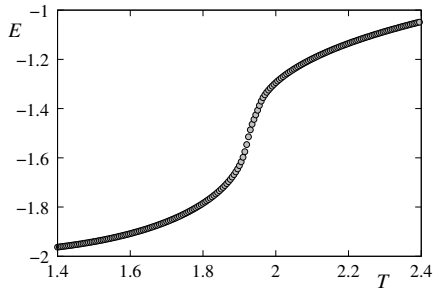

Figure 19. Energy versus temperature T for $L = 120$ for a 4-layer film.

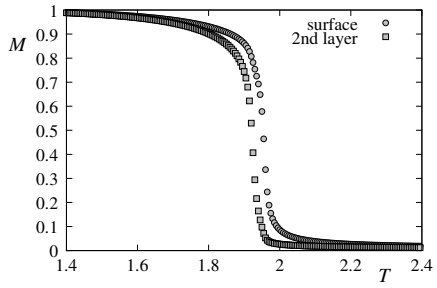

Figure 20. Layer magnetizations for $L = 120$ with a 4-layer film: the higher (lower) curve is the surface (beneath) layer magnetization.

5.1 Fully Frustrated XY Square Lattice

The fully frustrated with XY spins on the square lattice has been intensively studied [36-44]. The lattice with the ground-state (GS) spin configuration is shown in Fig. 26 (see [37]) where the angles between spins linked by a ferromagnetic (antiferromagnetic) bond is $\pi/4$ ($3\pi/4$) with right and left chiralities. This GS is equivalent to an Ising model on an antiferromagnetic square lattice. When T increases, one expects a transition of the Ising type. However, at finite T, the XY spins fluctuate around their GS orientations shown in Fig. 26, making the nature of the

phase transition more complex as seen below. Note that some authors have claimed that there are two separate transition of XY and Ising natures [41-44]. However, our results [36] and those of Refs. [39,40] show clearly that there is only a single transition of the new criticality called "coupled XY-Ising" universality class. We show below our results.

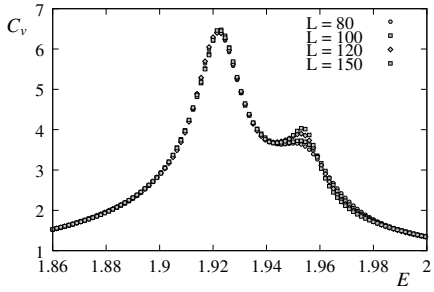

Figure 21. Specific heat are shown for various linear xy plane sizes L versus T for a 4-layer film.

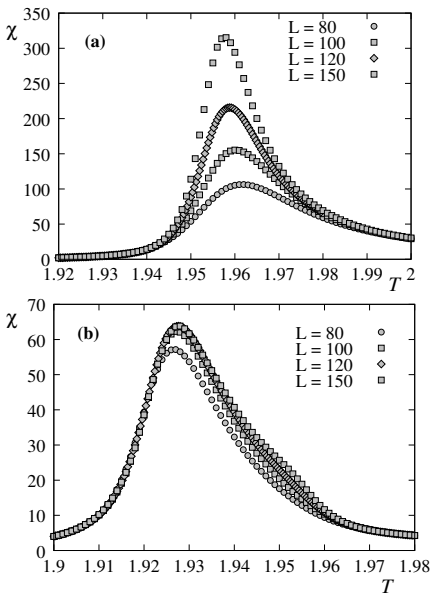

Figure 22. Susceptibilities of the first layer (a) and the second layer (b) are shown for various sizes L, versus T in a 4-layer film.

At the time of our work in Ref. [36], we did not calculate β and α as we have done on thin films presented in the preceding section. We were confident on the hyperscalings $d\nu = \gamma + 2\beta$ and $\alpha = 2 - d\nu$, so we used these relations to calculate β and α. However, in view of the question whether or not these relations are valid in particular cases such as the case of thin films shown in section 2 and the double transition in the case of fully frustrated square lattice presented here, we would like to check the validity of the hyperscaling relations. We can use ν and γ obtained here and the value of $2\beta/\nu = 0.31(3)$ obtained in Ref. [40], then we have $d\nu = 2 \times 0.852 = 1.704$ while $\gamma + 2\beta = 1.531 + 0.31 \times 0.852 = 1.795$. We see that $d\nu < \gamma + 2\beta$ even if we take into account errors of the exponents. Note that in these estimations we have used the Rushbrooke "equality" which is so far verified within errors in all known cases.

We note that it has been found in Ref. [40] by direct FSS that $\alpha/\nu = 0.48(7)$. Using $\nu = 0.852$ obtained by us and by Ref. [40], one obtains $\alpha \simeq 0.409$. This yields $2 - \alpha = 2 - 0.409 = 1.591$ which is not equal to $d\nu = 2 \times 0.852 = 1.704$ (here we do not use the Rushbrooke equality).

The conclusion for this coupled XY-Ising model based on the high-precision multi-histogram technique of our work and of Ref. [40] is that the hyperscaling relation is violated.

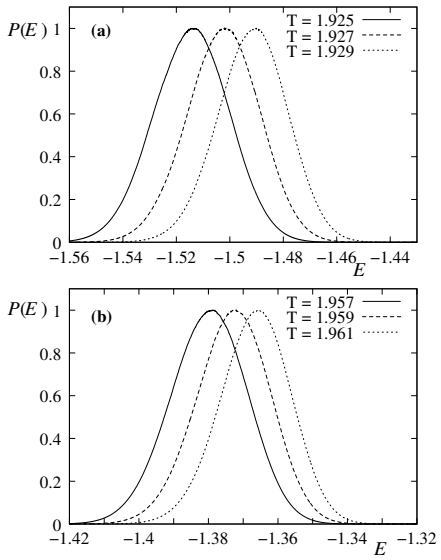

Figure 23. Energy histograms recorded at temperatures (indicated on the figure) corresponding to the the first (a) and second (b) peaks observed in the specific heat, for $L = 120$ with 4-layer film thickness $L_z = 4$.

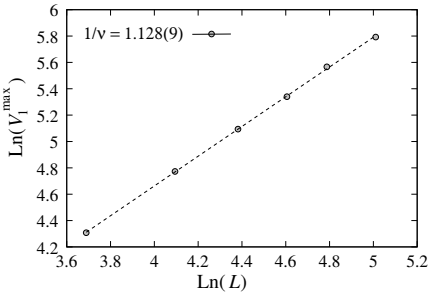

Figure 24. The maximum value of V_1 as a function of L in the ln – ln scale. The slope of this straight line gives $1/\nu$. The value of ν is $\nu = 0.887 \pm 0.009$.

Let us show the susceptibility versus T for $L = 44, 52, 60, 84, 100, 140$ in Fig. 28. A single peak for each size indicates a single transition as observed above. For $L = 140$ the peak is very close to $T_c(L = \infty) = 0.45522(2)$ estimated using Eq. (17) and $\nu = 0.852(2)$ calculated below using the maxima of V_1 and V_2 shown in Fig. 29. The fitting error is less than 0.1%. Note that our value is

the same as that of Ref. [40] which used the same multi-histogram MC technique, but differs from those obtained by less efficient methods ($\nu = 0.816$ in Ref. [43] and $\nu = 0.889$ in Ref. [44] for XY transition).

In Ref. [36], using the highly precise multi-histogram MC simulations described above, we have obtained the critical exponents ν and γ. We show in Fig. 27 the Binder energy cumulant U_E [15,16] as a function of L: as seen the curve approaches asymtotically 2/3 from below. This indicates a second-order nature of the transition.

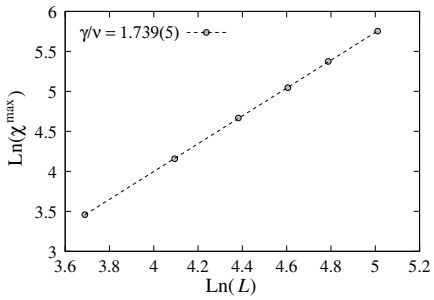

Figure 25. The maximum of the susceptibility $\chi^{\max}$ as a function of L in the ln – ln scale. The slope of this straight line gives γ/ν. The value of γ is $\gamma = 1.542 \pm 0.005$ using $\nu = 0.887 \pm 0.009$.

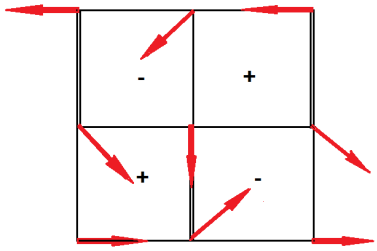

Figure 26. The square lattice: single (double) bonds are ferromagnetic (antiferromagnetic) bonds. The GS spin configuration is shown by red arrows. The right and left chiralities are denoted by "+" and "-"

5.2 Effect of magneto-elastic coupling on criticality

There are certainly other exotic models which may violate the hyperscaling relation for $d < 4$. One of these is the magneto-elastic coupling model that we have studied by using the multi-histogram technique [45,46]. The model consists of atoms on a stacked triangular lattice. Each atom carries an Ising spin and moves around its lattice equilibrium position. There are two kinds of interaction which are distance-dependent: the elastic interaction between atoms and the magnetic interaction between Ising spins. We suppose the following Hamiltonian:

$$\mathcal{H} = U_0 \sum_{i,j} J(r_{ij}) + U_m \sum_{i,j} J(r_{ij}) \sigma_i \sigma_j, \qquad (23)$$

where the first sum is the elastic interaction with amplitude U_0, and the second sum expresses the interacting spins with amplitude U_m. The distance-dependence is supposed to be the Lennard-Jones potential

$$J(r_{ij}) = (r_0/r_{ij})^{12} - 2(r_0/r_{ij})^6, \qquad (24)$$

where $r_0 = 1$ is the distance at equibrium betwenn NN in the triangular planes and also in the stacking direction., $r_{ij} = r_i - r_j$ is the instantaneous distance beween NN.

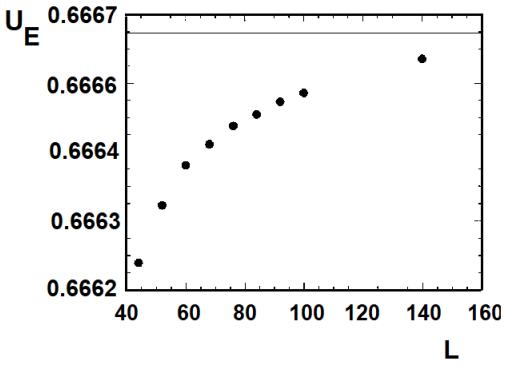

Figure 27. The Binder energy cumulant U_E versus L calculated at $T_c(L = \infty) = 0.4552(2)$. The horizontal line indicates $U_E(L = \infty) = 2/3$. The results show that the transition is of second order.

We calculate exponent γ using the peak values of χ for varying L. The curve in the ln – ln scale is shown in Fig. 30. The slope gives γ/ν. Using $\nu = 0.852$ we obtain $\gamma = 1.531(3)$ which is different from 1.448(24) obtained by Ref. [43].

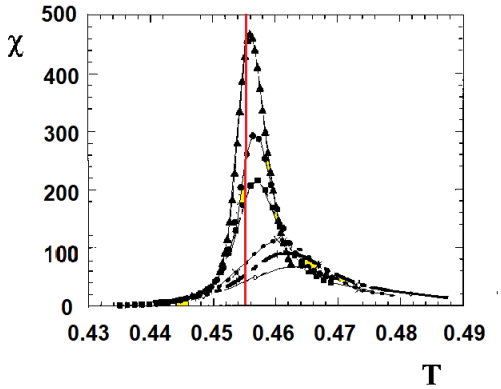

Figure 28. Susceptibility χ versus T for sizes $L = 44, 52, 60, 84, 100, 140$ (from lowest to highest curves). The red vertical line is the position of $T_c(L = \infty)$ calculated with Eq. (TCL) using ν obtained by Fig. 29 below.

In order to separate the spin disordering from the melting, we take the ratio $Q = U_0/U_m$ large enough so that the

magnetic transition occurs at low T. The cut-off distance is taken as $r_c = 1.366 r_0$.

Simulations using multiple histogram technique have been performed. The reader is referred to Ref. [45,46] for details. We just summarize the results in Table 2. Note that we have calculated at the time of our work (Ref. [45,46]) only ν and γ, and we have relied on the hyperscaling relations $d\nu = 2-\alpha$ and $\gamma/\nu = 2-\eta$ to calculate α and η listed in Table 2. Results from Ref. [47] are indicated by a in the Table and those taken from Ref. [48] are indicated by b However, we believe that if α is directly calculated as in section 2, the result of α may be different, due to the mixing of elastic and magnetic interactions. The nature of the transition depends on Q: it changes from the Ising nature at large Q to close to the XY universality class as seen in Table 2. In such complex situations, we are not sure that the hyperscaling relations are valid. Further direct calculations of α in the way we did in Ref. [18] are necessary to conclude on this point.

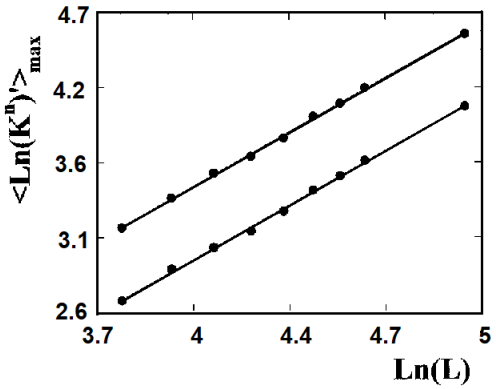

Figure 29. The maximum of cumulants V_1 and V_2 versus size

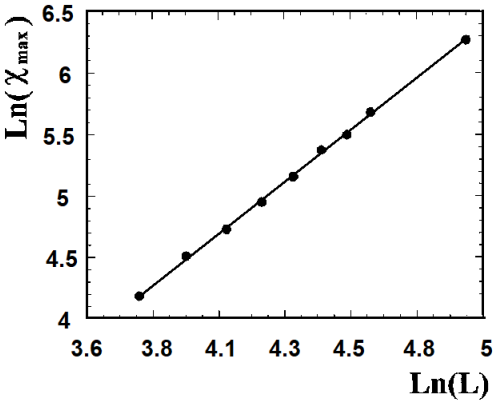

Figure 30. The maximum of susceptibility χ versus size $L = 44, 52, 60, 84, 100, 140$ in the $\ln - ln$ scale. The slope indicates the value of γ/ν. See text for the value of γ.

6 Concluding Remarks

We know that the hyperscaling relation is verified in $d = 3$ for Ising, XY and Heisenberg spins (results of highly efficient simulations), and in $d = 2$ for Ising spins (exact results). However, as shown in this paper, there are particular cases where the hyperscaling relation $d\nu = 2 - \alpha$ is violated. One of these situations is the case of a magnetic thin film with small thickness. To satisfy the hyperscaling relation, we have introduced the "effective dimension" whose value is non-integer between 2 and 3. However, the physical interpretation of this non-integer dimension may be a mere mathematical artifice, or it may be a reflection of a true fractal dimensionality of the system during the transition. Note that the hyperscaling relation is strictly defined for infinite systems. A more in-depth theoretical significance of d_{eff} needs to be clarified in the future. . Another case is the fully frustrated XY square lattice where we show that there is a single phase transition of a new coupled XY-Ising universality: the results of Ref. [40] and our results using the same method of simulation (multiple histogram technique) are the same for ν and γ. We did not calculated β, but we believe we should obtain the same β obtained in Ref. [40] in view of the same results obtained for ν and γ. The hyperscaling relation is then violated in this case. One may legitimately ask if this violation is not predictable since the standard scaling laws have been derived for pure systems. It fails to account for the combined energy-entropy equilibrium present in this case. The case of a system with a magneto-elastic interaction shows a new universality class. The possible violation of the hyperscaling relation in this case may be due to the fact the hyperscaling applies strictly to systems with short-range interactions, while this system has long-range off-lattice forces which can “effectively” alter the dimensionality of the system. This question needs further verifications.

To conclude, let us emphasize that, in view of the precise values we have obtained, the hyperscaling relation is not verified. We have also presented evidence of the violation of the hyperscaling relation in some other cases.

Finally, we note that while completing the present paper, we discover that the hyperscaling relation is also violated in the Kuramoto model with the random case (see [49]). The Kuramoto model is the 3D Ising model coupled with lattice vibrations. This case has some similarity with the magneto-elastic interaction model shown in our paper. The violation of the hyperscaling relation of the two cases may stem from the same ingredient: off-lattice long-range interaction.

The logical connection between the various “specific” systems studied in this paper as well as the Kuramoto model which violate the hyperscaling relation is that they do not obey the conditions in which the hyperscaling relation has been derived: infinite systems with a single order-parameter and a short-range interaction. We believe that more cases should be studied before a general conclusion could be drawn. This explains the question mark in the title of this paper.

Q	α	β	ν	γ	η
8	0.140(1)	0.310(1)	0.620(5)	1.245(5)	−0.01(1)
5	0.141(5)	0.301(5)	0.620(5)	1.259(5)	−0.03(1)
4	0.135(6)	0.308(5)	0.622(5)	1.249(5)	−0.01(1)
3D Ising	0.1070(*a*)	0.3265(*b*)	0.6305(*b*)	1.2390(*b*)	0.0370(*b*)
3	−0.024(4)	0.353(5)	0.675(5)	1.314(5)	0.053(5)
3D XY	−0.0100(*a*)	0.3455(*b*)	0.671(*b*)	1.3150(*b*)	0.040(*b*)

Table 2. Critical exponents obtained by multi-histogram technique for different Q. *a*: Results from Ref. [47], *b*: Results from Ref. [48]

The authors are grateful to X.-T. Pham-Phu and the late E. H. Boubcheur for participating in some works cited in this paper.

References

1. Diep, H. T. Frustrated Spin Systems: Emergence of a Modern Physics, *Comptes Rendus. Physique (France)* **2025** *26*, 225-251.
2. Diep, H. T. *Physics of Magnetic Thin Films: Theory and Simulation*, Jenny Stanford Publishing: New York, 2021 (600 pages).
3. Diep, H. T. *Theory of Magnetism-Application to Surface Physics*, World Scientific, World Scientific: Singapore, 2014.
4. Baxter, R. J. *Exactly Solved Models in Statistical Mechanics*, Academic Press Limited, London (U.K.) 1982.
5. Wilson, K. G. Renormalization Group and Critical Phenomena. I. Renormalization Group and the Kadanoff Scaling Picture *Phys. Rev. B* **1971** *4*, 3174.
6. Wilson, K. G. Renormalization Group and Critical Phenomena. II. Phase-Space Cell Analysis of Critical Behavior *Phys. Rev. B* **1971** *4*, 3184.
7. Fisher, M.E. The theory of critical point singularities. In Critical Phenomena, Proceedings of the 51st Enrico Fermi Summer School, Varenna; Green, M.S., Ed.; Academic Press: New York, NY, USA, **1971**; p. 1.
8. Fisher, M.E.; Barber, M.N. Scaling theory for finite-size effects in the critical region *Phys. Rev. Lett.* **1972**, *28*, 1516.
9. Cardy, J. *Scaling and renormalization in statistical physics*, Cambridge University Press: Cambridge (U.K.), 1996.
10. Berche, B.; Ellis, T.; Holovatch, Y.; Kenna, R. Phase transitions above the upper critical dimension *SciPost Phys. Lect. Notes* **2022**, *60*, 1.
11. Young, A. P. Violations of Hyperscaling in Finite-Size Scaling above the Upper Critical Dimension, *Entropy* **2024** *26(6)*, 509; https://doi.org/10.3390/e26060509.
12. Honchar, Yu.; Berche, B.; Holovatch, Yu.; Kenna, R. When correlations exceed system size: finite-size scaling in free boundary conditions above the upper critical dimension, *Condensed Matter Physics* **2024**, *27*, 13603:1-15.
13. Luijten, E. and Blöte, H.W.J. Finite-Size Scaling and Universality above the Upper Critical Dimensionality, *Phys. Rev. Lett.* **1996**, *76*, 1557.
14. O'Connor, D.; Stephens, C.R. ; Bray, A.J. Dimensional crossover in the large-N limit. *J. Stat. Phys.* **1997**, *87*, 273-291.
15. Ferrenberg, A. M. ; Swendsen, R. H. New Monte Carlo technique for studying phase transitions, *Phys. Rev. Let.* **1988** *61*, 2635. Erratum *Phys. Rev. Lett.* **1989** *63*, 1658.
16. Ferrenberg, A. M.; Swendsen, R. H. Optimized Monte Carlo data analysis, *Phys. Rev. Let.* **1989** *63*, 1195 .
17. A. Bunker, A.; Gaulin, B. D.; Kallin, C. Multiple-histogram Monte Carlo study of the Ising antiferromagnet on a stacked triangular lattice, *Phys. Rev. B* **1993** *48*, 15861-15872.
18. Pham-Phu, X.-T.; Ngo, V.-Thanh; Diep, H. T. Critical behavior of magnetic thin films, *Surface Science* **2009** *603*, 109–116.
19. Capehart, T. W.; Fisher, M. E. Susceptibility scaling functions for ferromagnetic Ising thin films, *Phys. Rev. B* **1976** *13*, 5021-5038.
20. Binder, K. The Monte Carlo Method for the Study of Phase Transitions: A Review of Some Recent Progress, *J. of Computational Physics* **1985** *59*, pp. 1-55.
21. Ferrenberg, A.M.; Landau, D.P. Critical behavior of the three-dimensional Ising model: A high-resolution Monte Carlo study, it Phys. Rev. B **1991** *44*, 5081-5091.
22. Diep, H. T.; Levy, J.C.S.; Nagai, O. Effects of Surface Spin Waves and Surface Anisotropy in Magnetic Thin Films at Finite Temperatures, *Phys. Stat. Solidi (b)* **1979** *93*, 351-361.
23. Diep, H.T. Temperature-Dependent Surface Magnetization and Critical Temperature of Ferromagnetic Thin Films, *Phys. Stat. Solidi (b)* **1981**, *103*, 809-815.
24. Diep, H. T. Quantum theory of helimagntic thin films, *Phys. Rev. B* **2015** *91*, 014436 (12 pp.).
25. El Hog, S.; Diep, H. T.; Puszkarski, H. Theory of magnons in spin systems with Dzyaloshinskii–Moriya interaction, *J. Phys.: Condens. Matter* **2017** *29* 305001 (10pp.).
26. Sharafullin, I.; Kharrasov, M. Kh.; Diep, H. T.

Dzyaloshinskii-Moriya interaction in magnetoferroelectric superlattices: Spin waves and skyrmions, *Phys. Rev. B* **2019** *99*, 214420 (14 pp.).
27. Schilbe, P.; Siebentritt, S.; and Rieder, K. H. Monte Carlo calculations on the dimensional crossover of thin Ising films *Phys. Lett. A* **1996** *216*, 20-25.
28. Pham-Phu, X. T.; Ngo, V. T.; Diep, H. T. Cross-Over from First- to Second-Order Transition in Frustrated Ising Antiferromagnetic Films, *Phys. Rev. E* **2009** *79*, 061106 (8 pp.).
29. Wang, F.; Landau, D.P. Efficient, Multiple-Range Random Walk Algorithm to Calculate the Density of States, *Phys. Rev. Lett.* **2001** *86*, 2050-2053.
30. Brown, G.; Schulhess, T. C. Wang–Landau estimation of magnetic properties for the Heisenberg model, *J. Appl. Phys.* **2005** *97*, 10E303.
31. Schulz, B. J.; Binder, K.; Müller, M.; Landau, D.P. Avoiding boundary effects in Wang-Landau sampling, *Phys. Rev. E* **2003** *67*, 067102 (2 pp.).
32. Malakis, A.; Martinos, S.S.; Hadjiagapiou, I.A.; Fytas, N.G.; Kalozoumis, P. Entropic sampling via Wang-Landau random walks in dominant energy subspaces, *Phys. Rev. E* **2005** *72*, 066120 (11 pp.).
33. Ngo, V. T.; Diep, H.T., Phase Transition in Heisenberg Stacked Triangular Antiferromagnets: End of a Controversy, *Phys. Rev. E* **2008** *78*, 031119.
34. Ngo, V.T.; Diep, H. T. Stacked Triangular XY Antiferromagnets: End of a Controversial Issue on the Phase Transition, *J. Appl. Phys.* **2008** *103*, 07C712.
35. Ngo, V.T. ; Hoang, D.-Tien; Diep, H. T. First-Order Transition in XY Fully Frustrated Simple Cubic Lattice, *Phys. Rev. E* **2010** *82*, 041123 (5 pages).
36. Boubcheur, E. H.; Diep , H. T. Critical behavior of the two-dimensional fully frustrated XY model, *Phys. Rev. B* **1998** *58*, 5163-5165.
37. Berge, B.; Diep , H. T. ; Ghazali, A.; Lallemand, P. Phase transitions in two-dimensional uniformly frustrated XYspin systems, *Phys. Rev. B* **1986** *34*, 3177-3184.
38. Granato, E.; Nightingale, M. P. Chiral exponents of the square-lattice frustrated XY model: a Monte Carlo transfer-matrix calculation, *Phys. Rev. B* **1993** *48*, 7438-7444.
39. Lee, J.; Kosterlitz, J. M.; Granato, E. Monte Carlo study of frustrated XY models on a triangular and square lattice, *Phys. Rev. B* **1991** *43*, 11531-11534.
40. Granato, E.; Kosterlitz, J.M.; Lee, J.; Nightingale, M. P. Phase transitions in coupled XY-Ising systems, *Phys. Rev. Lett.* **1991** *66*, 1090-1093.
41. Olsson, P. Two Phase Transitions in the Fully Frustrated XY Model, *Phys. Rev. Lett.* **1995** *75*, 2758-2761.
42. Jeon, G. S.; Park, S. Y.; Choi, M. Y. Double transitions in the fully frustrated XY model, *Phys. Rev. B* **1997** *55* 14088-14091.
43. Lee, S. ; Lee, K.C. Phase transitions in the fully frustrated XY model studied with use of the microcanonical Monte Carlo technique, *Phys. Rev. B* **1994** *49*, 15184-15189.
44. Ramirez-Santiago, G; Jose, J. V. Critical exponents of the fully frustrated two-dimensional XY model, *Phys. Rev. B***1994** *49*, 9567-9582.
45. Boubcheur, E. H.; Diep, H. T. Effect of elastic interaction on critical behavior of three-dimensional Ising model, *J. Appl. Physics* **1999** *85*, 6085-6087.
46. Boubcheur, E. H.; Massimino, P.; Diep, H. T. Effects of magnetoelastic coupling: critical behavior and structure deformation, *Journal of Magnetism and Magnetic Materials* **2001** *223*, 163-168.
47. Antonenko, S. A.; Sokolov, A. I. Critical exponents for a three-dimensional $O(n)$-symmetric model with $n > 3$, *Phys. Rev. E* **1995** *51*, 1894-1898.
48. Le Guillou, J. C.; Zinn-Justin, J. Accurate critical exponents from the ϵ-expansion, *J. Phys. (France) Lett.* **1985** *46*, L137-141.
49. Hong, H.; Chaté H.; Tang, L. ; Park, H. Finite-size scaling, dynamic fluctuations, and hyperscaling relation in the Kuramoto model, *Physical Review E* **2015** *92(2)*.